Physics of the Earth and Planetary Interiors 192–193 (2012) 68–80

Contents lists available at SciVerse ScienceDirect

Physics of the Earth and Planetary Interiors

journal homepage: www.elsevier.com/locate/pepi

Low viscosity of the bottom of the Earth's mantle inferred from the analysis of Chandler wobble and tidal deformation

Masao Nakada [a,*], Shun-ichiro Karato [b]

[a] Department of Earth and Planetary Sciences, Faculty of Science, Kyushu University, Fukuoka 812-8581, Japan
[b] Department of Geology and Geophysics, Yale University, New Haven, CT 06520, USA

ARTICLE INFO

Article history:
Received 22 April 2011
Received in revised form 30 August 2011
Accepted 13 October 2011
Available online 20 October 2011
Edited by George Helffrich

Keywords:
Chandler wobble
D″ layer
Viscosity
Tidal deformation
Maxwell body

ABSTRACT

Viscosity of the D″ layer of the Earth's mantle, the lowermost layer in the Earth's mantle, controls a number of geodynamic processes, but a robust estimate of its viscosity has been hampered by the lack of relevant observations. A commonly used analysis of geophysical signals in terms of heterogeneity in seismic wave velocities suffers from major uncertainties in the velocity-to-density conversion factor, and the glacial rebound observations have little sensitivity to the D″ layer viscosity. We show that the decay of Chandler wobble and semi-diurnal to 18.6 years tidal deformation combined with the constraints from the postglacial isostatic adjustment observations suggest that the effective viscosity in the bottom ~300 km layer is 10^{19}–10^{20} Pa s, and also the effective viscosity of the bottom part of the D″ layer (~100 km thickness) is less than 10^{18} Pa s. Such a viscosity structure of the D″ layer would be a natural consequence of a steep temperature gradient in the D″ layer, and will facilitate small scale convection and melt segregation in the D″ layer.

1. Introduction

Although it is well appreciated that rheological properties control a number of geodynamic processes, inferring rheological properties in the deep mantle is challenging. Two methods have been used to infer the rheological properties of Earth's mantle. One is to use the observed time-dependent deformation caused by the surface load such as the crustal uplift after the deglaciation (GIA: glacial isostatic adjustment) (Mitrovica, 1996), and another is to analyze gravity-related observations in terms of the density distributions inside of the mantle (Hager, 1984). The load causing GIA is relatively well constrained and hence GIA provides a robust estimate of mantle viscosity, but the GIA observations for the relative sea level (RSL) during the postglacial phase have little sensitivity to the viscosity of the mantle deeper than ~1200 km (Mitrovica and Peltier, 1991).

The latter approach can be applied to Earth's deep interior because density variation driving mantle flow can occur in the deep interior of the Earth and resultant gravity signals can be measured at the Earth's surface. In most cases, the density variation is estimated from the variation in seismic wave velocities. However, the estimation of density anomalies driving such a flow is difficult because the velocity-to-density conversion factor is not well constrained (Karato and Karki, 2001). This is particularly the case in the deep mantle where the temperature sensitivity of seismic wave velocities decreases due to high pressure (Karato, 2008). When chemical heterogeneity causes velocity heterogeneity, then even the sign of velocity-to-density conversion factor can change (Karato, 2008). Because the core–mantle–boundary has the large density contrast, it is a likely place for materials with different compositions (and hence densities) to accumulate (Lay et al., 1998). Consequently, a commonly used method to infer rheological properties from the seismic wave velocity anomalies is difficult to apply for these regions.

In this paper, we analyze two different data sets on time-dependent deformation, the observations on non-elastic deformation associated with Chandler wobble and tidal deformation to place new constraints on the rheological properties of the deep mantle. Deformation associated with Chandler wobble and tidal deformation occurs mostly in the deep mantle (Smith and Dahlen, 1981), and hence the analysis of these time-dependent deformations provides important constraints on the rheological properties of the deep mantle.

2. Time-dependent deformation associated with Chandler wobble and solid Earth tide

Many possible mechanisms of the excitation of Chandler wobble have been proposed (e.g., Munk and MacDonald, 1960; Lambeck, 1980; Smith and Dahlen, 1981). More recently, there is

* Corresponding author. Tel.: +81 92 642 2515; fax: +81 92 642 2684.
E-mail addresses: mnakada@geo.kyushu-u.ac.jp (M. Nakada), shun-ichiro.karato@yale.edu (S.-i. Karato).

0031-9201/$ - see front matter © 2011 Elsevier B.V. All rights reserved.
doi:10.1016/j.pepi.2011.10.001

growing consensus that a combination of atmospheric, oceanic and hydrologic processes, such as winds and variations in surface and ocean bottom pressure, is a dominant mechanism, although the relative contribution of each process is still controversial (see a review by Gross (2007)).

Once the Chandler wobble is excited, the amplitude of Chandler wobble decays with a decay time of $\tau_{CW} = 2Q_{CW}T_{CW}/2\pi$ in the absence of excitation, in which T_{CW} and Q_{CW} are the period and quality factor of Chandler wobble, respectively (e.g., Munk and Macdonald, 1960; Smith and Dahlen, 1981). However, because the details of the nature of excitation mechanism are unknown, two approaches have been used in estimating the values of T_{CW} and Q_{CW}. One is to employ a statistical model for the excitation (Wilson and Haubrich, 1976; Wilson and Vicente, 1990). The other is to employ certain excitation time series such as winds and pressure variations, and the T_{CW} and Q_{CW} are inferred by minimizing the power in Chandler wobble band of the difference between the given series and those derived from the observed polar motion and assumed T_{CW} and Q_{CW} (e.g., Furuya and Chao, 1996; Furuya et al., 1996; Aoyama and Naito, 2001; Gross et al., 2003; Gross, 2005).

Adopting the first approach, Wilson and Vicente (1990) considered a Gaussian random process for the excitation around the Chandler wobble frequency, and estimated T_{CW} and Q_{CW} based on the maximum likelihood method using the observed and simulated polar motion data spanning 86 years. Moreover, they performed Monte Carlo experiments to determine the corrections for the bias and standard errors of the estimates, and also demonstrated that the assumption for the excitation process is not critical. Their estimates recommended by Gross (2007) are: T_{CW} of 433 ± 1.1 (1σ) sidereal days and Q_{CW} of 179 with a 1σ range of 74–789, corresponding to the decay times of 30–300 years. Gross (2005), adopting the second approach based on several modeled excitation series with different data qualities for the duration and accuracy, showed that the data sets spanning at least 31 years are needed to obtain reliable estimates and the Q_{CW}-value is biased too low for inaccurate excitation series. We use T_{CW} and Q_{CW} estimated by Wilson and Vicente (1990).

Also, tidal deformations across the semi-diurnal to 18.6 years tides provide important constraints on the anelastic properties of the lower mantle (e.g., Lambeck and Nakiboglu, 1983; Sabadini et al., 1985; Wahr and Bergen, 1986; Ivins and Sammis, 1995; Dickman and Nam, 1998; Ray et al., 2001; Benjamin et al., 2006) or core–mantle coupling (e.g., Lambeck, 1980; Sasao et al., 1980) such as electromagnetic coupling (Buffett, 1992; Buffett et al., 2002).

In this paper, we first examine the validity of the Maxwell model based on the microscopic models of rheological properties of Earth materials. Then, we examine the decay time of Chandler wobble and tidal deformation and show that these deformations provide an important constraint on the viscosity structure of the D″ layer.

3. Rheological models: the Maxwell versus absorption band model

Time-dependent deformation such as the crustal uplift associated with GIA has often been analyzed using the Maxwell model (e.g., Peltier, 1974). This may be justified because for typical viscosities of 10^{20}–10^{22} Pa s, the Maxwell time is $\sim 10^{9}$–10^{11} s that is comparable to or smaller than the timescale of GIA ($\sim 10^{11}$ s). The timescales of time-dependent phenomena that we consider in this paper are much shorter, 10^{5}–10^{9} s. Consequently, the validity of the Maxwell model needs to be examined.

A commonly used model that includes both absorption band and viscous behavior is the Burgers model with distributed relaxation times (e.g., Jackson, 2007; Karato, 2008). The creep equation for such a model is given by

$$\varepsilon = \varepsilon_0 + At^{\alpha} + Bt \approx At^{\alpha} + Bt \tag{1}$$

where ε is strain, t is time, ε_0 is the instantaneous (elastic) strain, A and B are constants corresponding to transient and steady state creep respectively and α is a constant ($0 < \alpha < 1$) that depends on the distribution of relaxation times. When At^{α} term dominates, $Q \propto \omega^{\alpha}$, and when Bt term dominates, $Q \propto \omega$ (the Maxwell model behavior). In many materials microscopic elementary processes are common between steady-state and transient deformation (e.g., Amin et al., 1970) and therefore the activation enthalpy for both processes is nearly equal. This implies that if $B \propto \exp(-H^*/RT)$ then $A \propto \exp(-\alpha H^*/RT)$ (H^*: activation enthalpy). Therefore B is more sensitive to temperature than A, and hence the latter term dominates over the former at high temperature. Similarly Bt term dominates over At^{α} term at longer timescales (lower frequencies).

In experimental studies, it is often observed that when Q is parameterized as $Q \propto \omega^{\alpha}$, α is a constant ($\sim$0.3) for a broad range of frequency and temperature, but at low frequencies and high temperatures, α tends to be systematically larger (say $\sim$0.4–0.5 or higher) (e.g., Getting et al., 1997; Jackson and Faul, 2010). This can be explained by the increasing contribution of Bt term. Because $\alpha = \partial \log \varepsilon / \partial \log t$ (for $\varepsilon = At^{\alpha}$), it is easy to show that if α changes from 0.3 to 0.4–0.5, the contribution of Bt term is $\sim$40% for that of At^{α} term. The transition of α from 0.3 to 0.4–0.5 occurs (in olivine) at $T/T_m \sim 0.7$ and $\omega = 10^{-3}$ Hz, and we find that the contribution of the Bt term will be 500–1000% at $\omega = 10^{-5}$ Hz. Therefore we conclude that the Maxwell model will be a good approximation at tidal frequencies. A microscopic model to explain the evolution from the absorption band behavior to the Maxwell model behavior was presented by Karato and Spetzler (1990) and Lakki et al. (1998) based on dislocation unpinning. In addition, the viscosity of the region of interest is as low as $\sim 10^{18}$–10^{19} Pa s as we will show, then using the elastic modulus in that region of $\sim$300 GPa (PREM, Dziewonski and Anderson, 1981), the Maxwell time will be 3×10^{6}–3×10^{7} s (0.1–1 year), so at least for the Chandler wobble and 18.6 year tide, the Maxwell model is a good approximation.

Some previous studies used the absorption band model, $Q \propto \omega^{\alpha}$ with $\alpha \sim 0.3$, to interpret time-dependent deformation associated with tidal deformation and Chandler wobble (e.g., Smith and Dahlen, 1981; Benjamin et al., 2006). However, these authors, particularly Benjamin et al. (2006), used a physically inappropriate formula of the absorption band model that predicts an infinite Q at zero frequency (which is impossible from microscopic point of view: see Karato (1998), Karato (2010a) and Karato and Spetzler (1990)) and the transition to the Maxwell model at low frequency was not considered. Their observations can be explained by a model that includes the gradual transition to the Maxwell model behavior at $\omega = 10^{-5}$–10^{-6} Hz equally well.

Consequently, we examine the decay time of Chandler wobble and tidal deformation across the semi-diurnal to 18.6 years tides based on a Maxwell viscoelastic model (one parameter rheological model). Because temperature gradient is likely high in the D″ layer as inferred from the double-crossing of seismic rays of the phase boundary between perovskite and post-perovskite (Hernlund et al., 2005), the low viscosity layer is a natural consequence of a steep temperature gradient in the D″ layer.

4. Chandler wobble of a viscoelastic Maxwell earth

We estimate the decay time of Chandler wobble excited by the surface mass redistribution such as the variations in surface and ocean bottom pressure. Rotational responses on a Maxwell viscoelastic Earth due to the redistribution of surface mass are

computed by taking into account the conservation of angular momentum for the whole Earth, outer core and inner core (Nakada, 2006). The calculations include the effects of core–mantle couplings such as electromagnetic coupling (Nakada, 2009a) and gravitational torque acting on the inner core due to convective process (Buffett, 1997). However, we confirmed that these effects are negligible in simulating Chandler wobble on a viscoelastic Maxwell model (Nakada, 2011). That is, the solutions required in this study are the same as those obtained by a linearized Liouville equation generally used in the glacial isostatic adjustment, GIA (e.g., Sabadini and Peltier, 1981; Wu and Peltier, 1984; Mitrovica et al., 2005; Nakada, 2002, 2009b). Here we explain the method to evaluate the Chandler wobble due to surface load redistribution based on a linearized Liouville equation.

In an unperturbed state, the Earth rotates with an almost constant angular velocity Ω about the rotation axis. In the perturbed state, the angular velocity $\boldsymbol{\omega}$ can be written in terms of dimensionless small quantities m_1, m_2 and m_3 as $\boldsymbol{\omega} = \Omega(m_1, m_2, 1+m_3)$ (Munk and MacDonald, 1960; Lambeck, 1980). The quantities m_1 and m_2 describe the displacement of the rotation axis in the directions 0° and 90°E, respectively. Here we assume $|m_i| \ll 1$ as usually used for the Earth's rotation due to the GIA. Then, the Liouville equations describing the polar motion are given by (e.g., Sabadini and Peltier, 1981; Wu and Peltier, 1984; Mitrovica et al., 2005; Nakada, 2009b):

$$\frac{\dot{m}_1(t)}{\sigma_r} + m_2(t) = \frac{1}{C-A}(\delta(t) + k^L(t)) * \left(\Delta I_{23}(t) - \frac{\Delta \dot{I}_{13}(t)}{\Omega}\right) + \frac{k^T(t)}{k_f} * m_2(t) \quad (2)$$

$$-\frac{\dot{m}_2(t)}{\sigma_r} + m_1(t) = \frac{1}{C-A}(\delta(t) + k^L(t)) * \left(\Delta I_{13}(t) + \frac{\Delta \dot{I}_{23}(t)}{\Omega}\right) + \frac{k^T(t)}{k_f} * m_1(t) \quad (3)$$

where asterisk ($*$) denotes convolution, $\delta(t)$ is the delta function, $\sigma_r = (C-A)\Omega/A$, A and C are the equatorial and polar moments of inertia, respectively. $\Delta I_{13}(t)$ and $\Delta I_{23}(t)$ are forcing inertia elements for the polar motion. The degree-two ($n = 2$) surface load causing the polar motion is given by:

$$\sigma(\theta, \varphi, t) = \sigma_{211}(t)\cos\varphi P_{21}(\cos\theta) + \sigma_{212}(t)\sin\varphi P_{21}(\cos\theta) \quad (4)$$

Then the forcing inertia elements are given by $\Delta I_{13}(t) = -4\pi a^4 \sigma_{211}(t)/5$ and $\Delta I_{23}(t) = -4\pi a^4 \sigma_{212}(t)/5$ (e.g., Wu and Peltier, 1984), respectively. $P_{21}(\cos\theta)$ is the associated Legendre function with degree-two and order-one, and θ and φ represent the colatitude and E-longitude, respectively, and a is the mean radius of the Earth.

Love numbers $k^L(t)$ and $k^T(t)$ depend on the density and viscoelastic structure of the Earth, and characterize time-dependent Earth deformation to surface loading and that to the potential perturbation, respectively (Peltier, 1974). k^f is the fluid Love number characterizing the hydrostatic state of the Earth and is defined by $3G(C\text{-}A)/(a^5\Omega^2)$, where G is the gravitational constant (Munk and MacDonald, 1960). Although it may be necessary to modify the term of k^f for the Earth with excess flattening inferred from non-hydrostatic geoid (Mitrovica et al., 2005; Nakada, 2009b), the effects are negligibly small in simulating Chandler wobble and neglected here. Consequently, we assume $\sigma_{211}(t)$, $\sigma_{212}(t)$ and the density and viscoelastic structure of the Earth, then we can compute $m_1(t)$ and $m_2(t)$ by solving Eqs. (2) and (3). The solutions for the GIA indicate that Chandler wobble is superimposed on the secular polar motion (Nakada, 2009b), consistent with the observations of the polar motion qualitatively (e.g., Lambeck, 1980).

Here we assume $\sigma_{212}(t) = 0$, and, for a simplicity, consider a forcing function for $\sigma_{211}(t)$ such that the surface load linearly increases for $0 \leqslant t \leqslant 0.1$ years from zero to $\sigma_{211}(0.1) = 93.6\ \mathrm{kg\ m^{-2}}$ and linearly decreases for $0.1 \leqslant t \leqslant 0.2$ years and that for $t \geqslant 0.2$ years is zero. The value at $t = 0.1$ years is adopted by taking into account the observed average amplitude of the Chandler wobble of ~0.2 arc second (e.g., Lambeck, 1980) but this value does not affect the relaxation time.

5. Decay time of the predicted Chandler wobble and plausible viscosity models

In this study, we use the PREM (Dziewonski and Anderson, 1981) model for the density and elastic constants, and the response is elastically compressible. As a background rheological structure, we use a model referred to as R0 here (Fig. 1) with 100 km elastic lithosphere, upper mantle viscosity of 10^{21} Pa s and lower mantle viscosity of 10^{22} Pa s. This model explains the sea-level variations for the postglacial rebound around the Australian region (Nakada and Lambeck, 1989). The choice of the background model does not affect the conclusions on the viscosity of the bottom layer of the mantle so much.

Predicted amplitude of m_1 for R0 (Fig. 2) decays insignificantly for $0 \leqslant t \leqslant 40$ years and the decay time (τ_{CW}) for R0 estimated from the peak values shown in Fig. 2 is ~2600 years, inconsistent with the observed significant attenuation. In order to reproduce the observed large attenuation for Chandler wobble with a R0-type model, one needs to reduce the viscosities to the extent that violates the constraints by GIA observations for the relative sea-level (RSL). Consequently, we investigate the effects of a low viscosity layer (LVL) in six different zones on the decay of Chandler wobble, i.e. 100–400 km depth (R1), 400–670 km depth (R2), 791–1091 km depth (R3), 1691–1991 km depth (R4), 2591–2891 km depth (R5) and 2741–2891 km depth (R6) (Fig. 1 and Table 1). For each model, we will seek models that explain the decay times (or attenuation) of Chandler wobble without violating GIA constraints by RSL observations (see Appendix A for RSL variations for viscosity models with LVL in the lower mantle). The LVL for R1 corresponds to the asthenosphere beneath the lithosphere, and R2 is adopted because the transition zone might be a LVL due to the influence of water (Karato, 2011). Models R3 and R4 are adopted to examine the sensitivity of τ_{CW} to the LVL of the lower mantle. Models R5 and R6 are adopted to examine the trade-off between the viscosity ($\eta_{D''}$) and

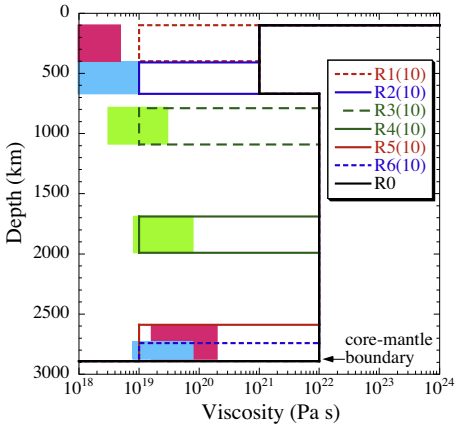

Fig. 1. A base-line viscosity model R0, and models R1(10), R2(10), R3(10), R4(10), R5(10) and R6(10) with a LVL of 10×10^{18} Pa s in certain regions (see Table 1). The thickness of elastic lithosphere for these models is 100 km. We adopt low viscosity models with $(1, 2, 5, 10, 20, 50, 100) \times 10^{18}$ Pa s. The shaded region for each model shows the viscosity range inferred from the decay of Chandler wobble (Fig. 5).

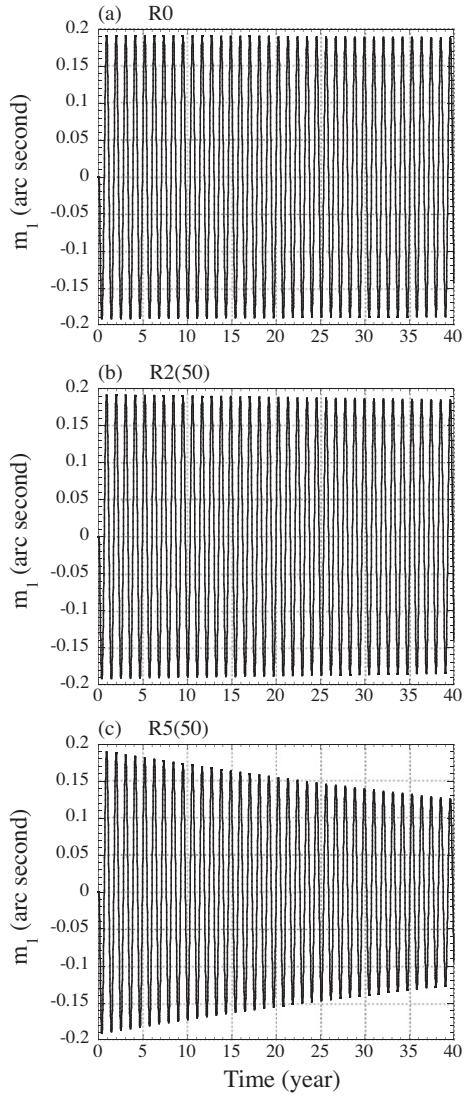

Fig. 2. Predictions of m_1 for viscosity models R0, R2(50) and R5(50). The amplitudes for models R0 and R2(50) decay insignificantly for a period of $0 \leqslant t \leqslant 40$ years. That for R5(50), with a low viscosity of 5×10^{19} Pa s for 2591–2891 km depth, shows a significant decay for $0 \leqslant t \leqslant 40$ years.

thickness ($H_{D''}$) of the LVL at the base of the mantle. We consider various viscosities of the LVL, $(1, 2, 5, 10, 20, 50, 100) \times 10^{18}$ Pa s (see Table 1).

Predictions of m_1 for viscosity models R0, R2(50) and R5(50) are shown in Fig. 2. A viscosity model R2(50) has a low viscosity layer of 5×10^{19} Pa s for 400–670 km depth, and R5(50) has a low viscosity layer of 5×10^{19} Pa s for 2591–2891 km depth. The predicted amplitude for R0 and R2(50) is about 0.2 arc second and decays insignificantly for a period of $0 \leqslant t \leqslant 40$ years, but that for R5(50) shows a significant decay for $0 \leqslant t \leqslant 40$ years. The difference of the decay of Chandler wobble is attributed to the relaxational behavior characterized by Love numbers as discussed below. In this study, we adopt a model of R0 as a background rheological structure. However, we obtain a similar conclusion on the decay time even if we adopt the models obtained by GIA for European regions (Lambeck et al., 1996), or by the flow models derived from global long geoid anomalies (Hager et al., 1985) or by the joint inversions of GIA and convection data sets (Mitrovica and Forte, 2004) compiled by Forte (2007).

The effects of a low viscosity layer can be examined by looking at the time-dependent response to a step-wise loading function,

Table 1
Viscosity models (R1–R6) with a low viscosity layer (LVL) in the mantle. The viscosities of the LVL are $(1, 2, 5, 10, 20, 50, 100) \times 10^{18}$ Pa s. The number of the parenthesis in the third column (Abbreviation of each LVL model) indicates the number of i for the LVL viscosity of $i \times 10^{18}$ Pa s. In these models, the lithospheric (elastic) thickness is 100 km, and the upper and lower mantle viscosities except for the LVL are 10^{21} and 10^{22} Pa s, respectively.

Model name	Depth range of LVL (km)	Abbreviation of each LVL model
R1	100–400	R1(1), R1(2), R1(5), R1(10), R1(20), R1(50), R1(100)
R2	400–670	R2(1), R2(2), R2(5), R2(10), R2(20), R2(50), R2(100)
R3	791–1091	R3(1), R3(2), R3(5), R3(10), R3(20), R3(50), R3(100)
R4	1691–1991	R4(1), R4(2), R4(5), R4(10), R4(20), R4(50), R4(100)
R5	2591–2891	R5(1), R5(2), R5(5), R5(10), R5(20), R5(50), R5(100)
R6	2741–2891	R6(1), R6(2), R6(5), R6(10), R6(20), R6(50), R6(100)

Heaviside Love numbers, defined by $k^{L,H}(t) = k^{L}(t) * H(t)$ and $k^{T,H}(t) = k^{T}(t) * H(t)$, in which $H(t)$ is the Heaviside function (Peltier, 1974). These Love numbers characterize the relaxational behavior of the Earth to the forcing with Heaviside function (Peltier, 1974). Fig. 3 illustrates $k^{T,H}(t)$ calculated for each viscosity model for $10^{-3} \leqslant t \leqslant 10^{3}$ years. The LVL for R1 and R2 affects the relaxation rather uniformly for a whole time range. The behavior may be interpreted as the response for a model that the average viscosity is smaller than that for R0 because of LVL. The LVL just above the core for R5 and R6 affects only for $t < 100$ years and the change of $k^{T,H}(t)$ for the period ($\Delta k^{T,H}$) is approximately proportional to the thickness ($\Delta k^{T,H} \propto H_{D''}$), suggesting that the relaxation is confined to the low viscosity zone. The relaxation behavior for R3 and R4 is intermediate between that for R1–R2 and R5–R6. Fig. 4 also shows the predicted $k^{L,H}(t)$ for R1–R6 with viscosities of 10^{18}, 10^{19} and 10^{20} Pa s for the low viscosity layer and R0. The time range for these plots is $10^{-3} \leqslant t \leqslant 10^{4}$ less than the timescale of post-glacial rebound. The characteristics are similar to those for $k^{T,H}(t)$ shown in Fig. 3 for these viscosity models. It is expected that the decay of Chandler wobble would reflect the characteristic relaxation behavior for each viscosity model.

We also estimated the relaxation time using the predictions of Chandler wobble (Fig. 2). Fig. 5 illustrates the relaxation times for R1–R6 as a function of the viscosity of LVL (see also Fig. 1). Those for Q_{CW} of 74, 179 and 789 are 28, 68 and 298 years, respectively. The viscosity of the LVL for $Q_{CW} = 179$ is $\sim 4 \times 10^{19}$ Pa s for R5 with 300 km thickness and $\sim 2 \times 10^{19}$ Pa s for R6 with 150 km thickness. Our numerical experiments approximately indicate $\tau_{CW} \propto \eta_{D''}/H_{D''}$, which is also applicable to models with LVL in the lower mantle. The viscosity for R6 will have a range of $(0.7–9) \times 10^{19}$ Pa s considering the 1σ uncertainty for Q_{CW}. That for R5 is $10^{19} < \eta_{D''} < 2 \times 10^{20}$ Pa s, consistent with $\tau_{CW} \propto \eta_{D''}/H_{D''}$.

The relaxation times of 30–300 years are explained by viscosity models with a significantly low viscosity of 10^{18}–10^{19} Pa s for 100–400 km or 400–670 km depth. Significant low viscosity zone shallower than ~1200 km depth such as R1–R3 is, however, inconsistent with the viscosity structure derived from GIA observations for RSL and other geophysical studies (Forte, 2007). Also, the low viscosity for the mid-lower mantle smaller than $\sim 10^{20}$ Pa s such as R4 would be excluded from studies using non-hydrostatic geoid and flow models (Hager et al., 1985) and a joint inversion of GIA and convection data sets indicating 10^{23} Pa s around ~2000 km depth (Mitrovica and Forte, 2004). Therefore, we conclude that the low viscosity regions are needed to explain the observed Q_{CW} in somewhere in the deep mantle. The depth range is not well constrained by the present analysis because of the trade-off between

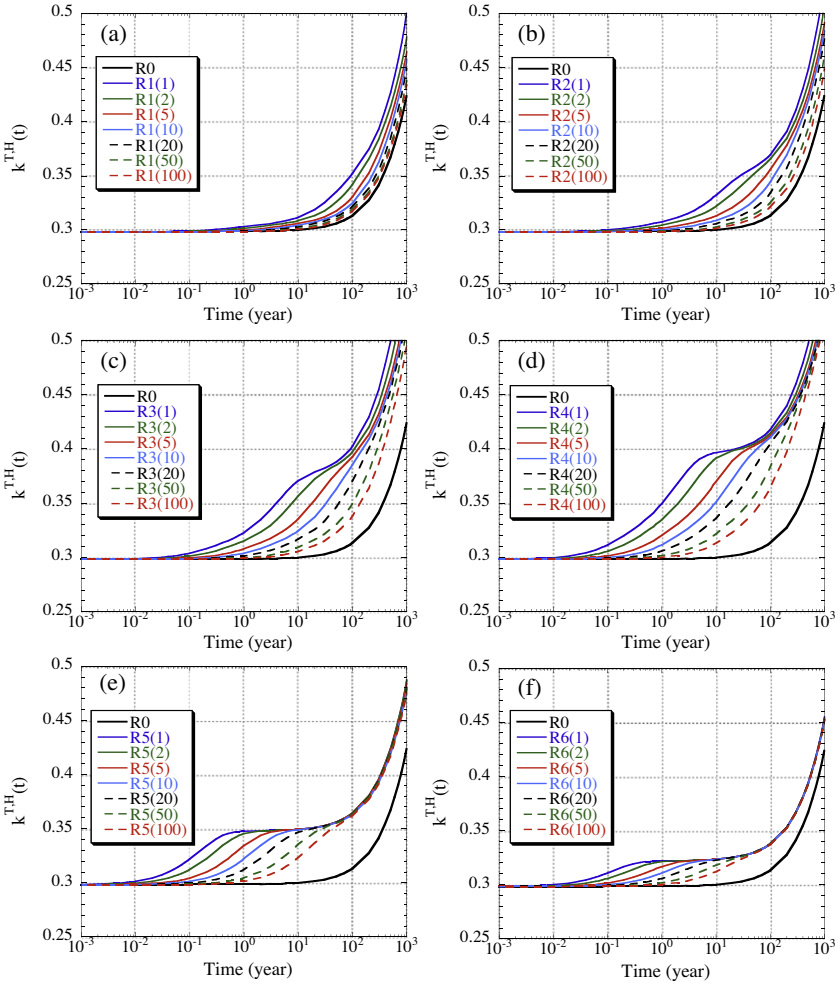

Fig. 3. Heaviside Love numbers $k^{T,H}(t)$ (Peltier, 1974) for a time range of $10^{-3} \leqslant t \leqslant 10^{3}$ years based on viscosity models R0, R1, R2, R3, R4, R5 and R6 (see Table 1) characterizing the relaxation behavior of the Earth to the potential perturbation with a step-wise function.

viscosity and the thickness of the LVL. However, if we accept models of high lower mantle viscosity such as the models compiled by Forte (2007), it is likely that this low viscosity layer is in the deep regions of the lower mantle.

Because temperature gradient is likely high in the D″ layer as inferred from the double-crossing of seismic rays of the phase boundary between perovskite and post-perovskite (Hernlund et al., 2005), we consider that this low viscosity layer is likely the D″ layer. We evaluate the viscosity reduction for various temperature-depth profiles in the D″ layer using a relation of $\eta \propto \exp(H^*/RT)$, where η is the viscosity and H^* is the activation enthalpy (~500 kJ/mol (Yamazaki and Karato, 2001)). The temperature just above the D″ layer is assumed to be adiabatic. With a plausible temperature increase, substantial drop of viscosity can be explained (inset of Fig. 5). There was a suggestion that the D″ layer might have low viscosity due to the intrinsic weakness of the post-perovskite (Ammann et al., 2010). However, their results (Ammann et al., 2010) cannot be justified from the materials science viewpoint (Karato, 2010b).

6. Constraint on viscosity structure of D″ layer from tidal deformation of the Earth

The proposed low viscosity layer is also consistent with the time-dependent tidal deformation. The deformation to a luni-solar tidal force is sensitive to the anelastic properties of deep mantle (Smith and Dahlen, 1981), and may be discussed based on the Maxwell viscoelastic model (Lambeck and Nakiboglu, 1983; Sabadini et al., 1985; Ivins and Sammis, 1995). That is, we examine the deformations to a luni-solar tidal force and the centrifugal force variations accompanying Chandler wobble. The forcings are given by $F(\omega, t) \propto e^{i\omega t}$ as a function of frequency ω. Here we do not consider the effects of the core–mantle coupling such as electromagnetic coupling (Buffett, 1992; Buffett et al., 2002). Then the response, $R(\omega,t)$, is evaluated by $R(\omega, t) = k^T(t) * F(\omega, t)$ using the tidal Love number $k^T(t)$ as inferred from the Heaviside Love number (Peltier, 1974), and given by $k^{T,P}(\omega)F(\omega, t)$ (Lambeck and Nakiboglu, 1983; Sabadini et al., 1985). The Love number, $k^{T,P}(\omega)$, takes a complex form of $k^{T,P}(\omega) = k_r^{T,P}(\omega) + ik_i^{T,P}(\omega)$, and depends on the viscoelastic structure, particularly on the viscosity structure of the deep mantle. The amplitude of the response is characterized by its modulus, $|k^{T,P}|$, and the phase difference between the response and forcing, $\Delta\phi$, is given by $\Delta\phi = \tan^{-1}\left(-k_i^{T,P}/k_r^{T,P}\right)$. Consequently, geodetic observations make it possible to estimate the Love Number as a function of the frequency by analyzing the time series data of $R(\omega,t)$. The frequency-dependent responses to the forcings are estimated regardless of the rheology of the solid Earth, and we interpret the estimates in terms of the Maxwell viscoelastic model.

Fig. 6 illustrates the predictions for R0 and R1–R6 and geodetically-inferred Love numbers for semi-diurnal (M_2) (Ray et al., 2001), nine-day (M_9) (Dickman and Nam, 1998), fortnightly (M_f) (Dickman and Nam, 1998; Benjamin et al., 2006), monthly (M_m) (Dickman and Nam, 1998; Benjamin et al., 2006), 18.6 years tides (Benjamin et al., 2006) and Chandler wobble corrected for the

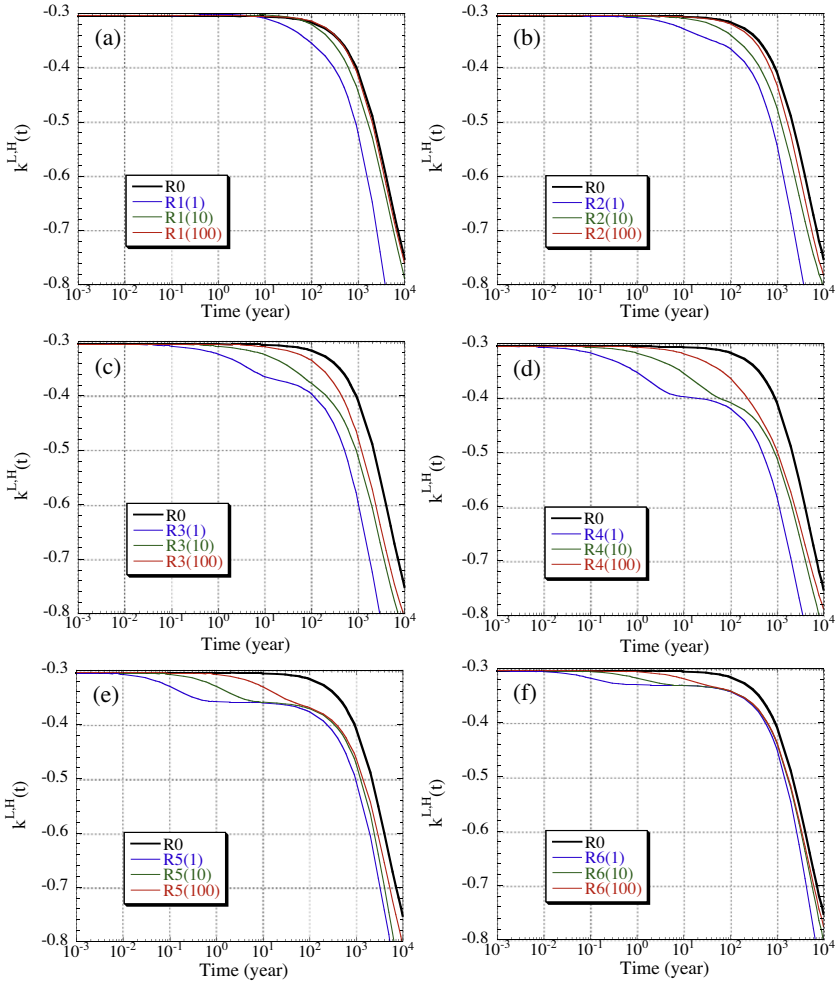

Fig. 4. Predictions of $k^{L,H}(t)$ (Peltier, 1974) for a time range of $10^{-3} \leqslant t \leqslant 10^{4}$ years based on viscosity models R1, R2, R3, R4, R5 and R6 with low viscosities of 10^{18}, 10^{19} and 10^{20} Pa s, and for R0 (see Table 1). The detailed behavior of predicted $k^{T,H}(t)$ for a time range of $10^{-3} \leqslant t \leqslant 10^{3}$ is shown in Fig. 3 for these viscosity models.

ocean effects (Dickman and Nam, 1998; Benjamin et al., 2006) as a function of the period (T). The estimates for Chandler wobble correspond to the response to the accompanying variations in centrifugal force (Dickman and Nam, 1998; Benjamin et al., 2006). The estimates for 18.6 years tide (Benjamin et al., 2006) are derived from the degree-two and order-zero gravity component for satellite laser ranging from 1979 to 2004. These data include the effects associated with atmospheric, oceanic and hydrologic processes. The left, middle and right estimates are corrected for atmospheric effects, atmospheric and ocean circulation effects, and atmospheric, ocean circulation and continental water + snow + ice effects, respectively (Benjamin et al., 2006).

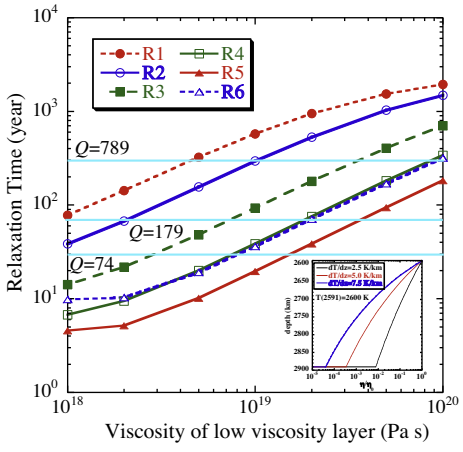

Fig. 5. Relaxation times of Chandler wobble for viscosity models R1, R2, R3, R4, R5 and R6 as a function of the viscosity of LVL (see Table 1). The inferred viscosity ranges for $74 \leqslant Q_{CW} \leqslant 789$ (Wilson and Vicente, 1990) are also shown in Fig. 1. The inset illustrates viscosity-depth profiles with temperature gradients of 2.5, 5.0 and 7.5 K km^{-1}. η is viscosity and η_0 is the viscosity at the top of the D″ using the activation enthalpy of 500 kJ mol^{-1} (Yamazaki and Karato, 2001) and T(2591) = 2600 K.

The predictions of R0 for $T < 20$ years with $k_r^{T,P} \simeq k_r^{T,P}(0)$ and $k_i^{T,P} \simeq 0$ imply that the response is nearly elastic. The predictions for R1 and R2 with a low viscosity layer in the upper mantle cannot explain most of the geodetically-inferred Love numbers. The predictions based on the preferred models for R5 explain the estimates for 18.6 years tide, but not those for M_f, M_m and Chandler wobble, particularly for the real parts characterizing the amplitude because of $|k^{T,P}| \simeq k_r^{T,P}$. The tendency for the predictions for R3 and R4 with a low viscosity layer of smaller than 10^{19} Pa s in the lower mantle is similar to that for R5 discussed above.

However, if we introduce a hybrid model, D2a, which has the viscosity of 5×10^{19} Pa s for the upper 200 km and 10^{17} Pa s for the lower 100 km thickness (see inset of Fig. 7 and Table 2), then we can explain both CW and tidal observations. Fig. 7 shows the predictions for two-layer low viscosity models at the bottom of the mantle (D2a–D2g in Table 2). The viscosity for the upper 200 km thickness is

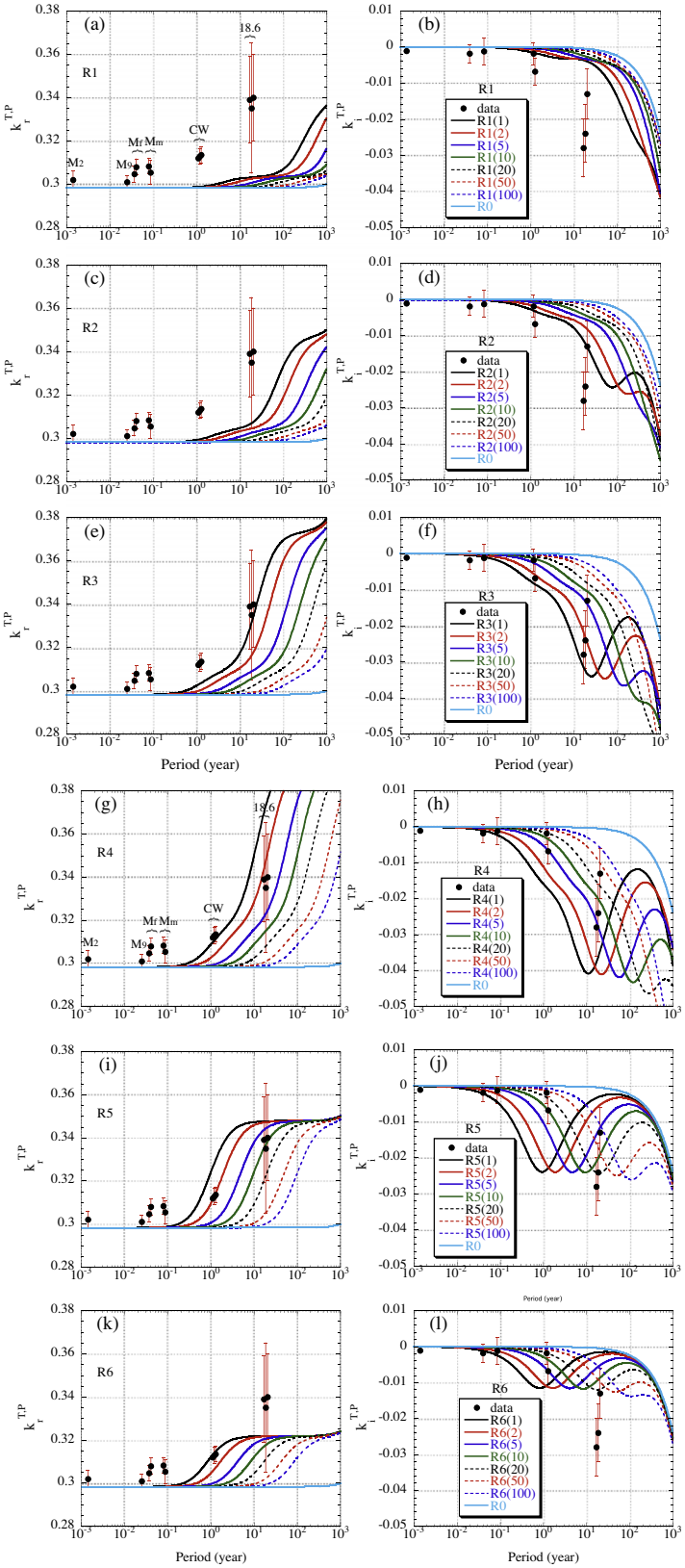

Fig. 6. Real (a, c, e, g, i, k) and imaginary (b, d, f, h, j, l) parts for predicted Love numbers for R0, R1–R6 caused by the periodic forcings and geodetic-derived values for semi-diurnal (M_2) (Ray et al., 2001), nine-day (M_9) (Dickman and Nam, 1998), fortnightly (M_f) (Dickman and Nam, 1998; Benjamin et al., 2006), monthly (M_m) (Dickman and Nam, 1998; Benjamin et al., 2006, Chandler wobble (Dickman and Nam, 1998; Benjamin et al., 2006) and 18.6 years tides (Benjamin et al., 2006) as a function of the period (T). To clearly show each estimate, we plot the data with appropriate shift of position of the period. We comment about the three estimates for 18.6 years tide (Benjamin et al., 2006). These estimates were derived from the degree two ($n = 2$) and order zero ($m = 0$) gravity component for satellite laser ranging (SLR) from 1979 to 2004 (26 years). These data include the effects associated with atmospheric, oceanic and hydrologic processes. The left, middle and right estimates are corrected for atmospheric effects, atmospheric and ocean circulation effects, and atmospheric, ocean circulation and continental water + snow + ice effects, respectively (Benjamin et al., 2006).

5×10^{19} Pa s, and the viscosity for the lower layer with 100 km thickness is variable, 10^{17}–10^{19} Pa s. For example, the viscosity of the lower layer for a model of D2b is 2×10^{17} Pa s. The predictions for R5(10), R5(20) and R5(50) cannot explain the estimates for M_f, M_m and Chandler wobble, particularly for the real parts characterizing the amplitudes. However, models with the viscosity smaller than 5×10^{17} Pa s are rather consistent with the geodetically-inferred values. The thickness of the lower layer with 100 km is adopted by taking into account the relationship of $\Delta k^{T,H} \propto H_{D''}$ inferred from the $k^{T,H}(t)$ for the viscosity models R5 and R6 (see Fig. 3e and f). The value of $k_r^{T,P}(T)$ at $T \sim 1$ year is consistent with the prediction for the model with the thickness of ~100 km. That is, the deformation for $T < 10$ years is significantly sensitive to the viscosity and the thickness of the lower layer. Such a depth-dependent viscosity is a natural consequence of a steep temperature gradient in the D″ layer (inset of Fig. 7). We conclude that the observations on Earth deformation caused by the tidal forcings and the decay of CW may provide useful constraints on the viscosity structure of the D″ layer, and that the bottom of Earth's mantle has much lower viscosity than the rest of the lower mantle.

We examine the sensitivity of the relaxation time of Chandler wobble, τ_{CW}, to the two-layer low viscosity models. Here we denote the viscosity and thickness of the bottom layer by η_b and H_b, respectively. Fig. 8 shows the relaxation times for two models with $H_b = 50$ and 100 km. The total thickness of the low viscosity zone is 300 km, and the viscosity of the upper layer is 5×10^{19} Pa s. The models with $H_b = 100$ km (D2a–D2g in Table 2) are the same as those adopted for the Love numbers in Fig. 7. In both models, the relaxation times for $\eta_b < 10^{18}$ Pa s decrease with increasing η_b and those for $\eta_b > 2 \times 10^{18}$ Pa s increase with increasing η_b. The minimum values are ~10 years at $\eta_b \sim 10^{18}$ Pa s.

In models with $H_b = 100$ km, the relaxation time for $\eta_b \sim 10^{17}$ Pa s is similar to that for $\eta_b \sim 2 \times 10^{19}$ Pa s. This probably reflects that the lower layer with a viscosity smaller than $\sim 10^{17}$ Pa s behaves as an inviscid layer to the deformation associated with the decay of Chandler wobble, and the response is mainly determined by the upper layer with viscosity of 5×10^{19} Pa s. With increasing η_b, the lower layer affects the deformation for Chandler wobble, and the decay time decreases and takes a minimum value at $\eta_b \sim 10^{18}$ Pa s. As the viscosity of the lower layer increases from $\eta_b \sim 2 \times 10^{18}$ Pa s, the effective viscosity of the two-layer model increases resulting in the increase of the decay time of Chandler wobble. In models with $H_b = 100$ km, therefore, models with $\eta_b < 3 \times 10^{17}$ Pa s and $\eta_b > 6 \times 10^{18}$ Pa s explain the decay time of Chandler wobble, but models with $3 \times 10^{17} < \eta_b < 6 \times 10^{18}$ Pa s cannot explain the decay time. That is, two-layer low viscosity models with $\eta_b < 3 \times 10^{17}$ Pa s, rather consistent with the geodetically-inferred Love numbers (Fig. 7), also explain the decay time of Chandler wobble derived from the $74 \leqslant Q_{CW} \leqslant 789$.

Table 2
Two layer low viscosity models for the D″ layer (2591–2891 km depth). In these models, the lithospheric (elastic) thickness is 100 km, upper mantle viscosity is 10^{21} and the lower mantle viscosity except for the D″ layer is 10^{22} Pa s.

Model name	Viscosity for the upper layer of 2591–2791 km depth (Pa s)	Viscosity for the lower layer of 2791–2891 km depth (Pa s)
D2a	5×10^{19}	1×10^{17}
D2b	5×10^{19}	2×10^{17}
D2c	5×10^{19}	5×10^{17}
D2d	5×10^{19}	1×10^{18}
D2e	5×10^{19}	2×10^{18}
D2f	5×10^{19}	5×10^{18}
D2g	5×10^{19}	1×10^{19}

7. Secular variations of the Earth's rotation due to GIA for viscosity model with low viscosity D″ layer

The GIA observations for the RSL have little sensitivity to the viscosity of the mantle deeper than ~1200 km depth (Mitrovica and Peltier, 1991), but the rotational variations of the Earth due to GIA, a secular polar wander of the rotation pole (true polar wander) and a non-tidal acceleration of the rate of rotation, are sensitive to the viscosity structure of the deep mantle (e.g., Wu and Peltier, 1984). However, the observations for the Earth's rotation are also affected by the present-day melting events of polar ice sheets and mountain glaciers (e.g., Peltier, 1988; Nakada and Okuno, 2003; Mitorovica et al., 2006) and convective processes in the mantle (e.g., Ricard and Sabadini, 1990; Steinberger and O'Connell, 1997; Nakada, 2009b). For example, the observed polar wander of $\sim 1^\circ\,\mathrm{Myr}^{-1}$ towards Hudson Bay (Dickman, 1977; McCarthy and Luzum, 1996) and the rate of change of the degree-two zonal harmonics of the Earth's geopotential, $\dot{J}_2$, with $\sim(2.5\text{–}3.0) \times 10^{-11}\,\mathrm{yr}^{-1}$ (Nerem and Klosko, 1996) are contributed by these processes (GIA, present-day melting events and mantle convection), and it is difficult to extract the GIA contribution only from these observations. However, there is no doubt that these signals include important information on the lower mantle viscosity structure. From this viewpoint, many studies have examined the sensitivities of these rotational signals to the average lower mantle viscosity (e.g., Sabadini and Peltier, 1981; Wu and Peltier, 1984; Nakada, 2002). Here we show some showing the sensitivity of

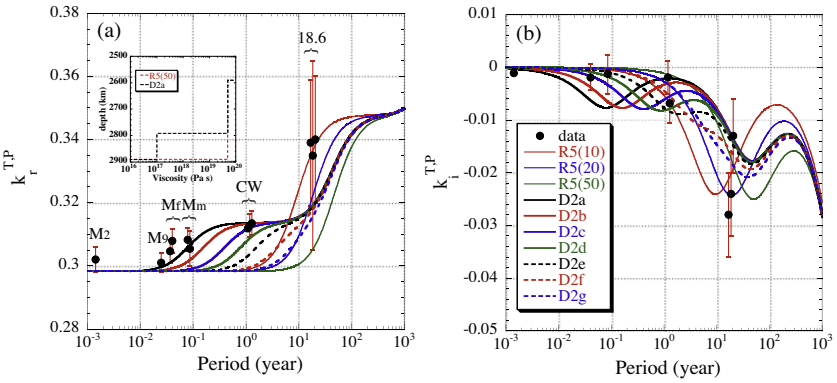

Fig. 7. Real (a) and imaginary (b) parts for predicted Love numbers for R5 and its modified two-layer low viscosity models (D2a–D2g in Table 2) caused by the periodic forcings and geodetically-inferred values for semi-diurnal (M_2), nine-day (M_9), fortnightly (M_f), monthly (M_m), Chandler wobble and 18.6 years tides as a function of the period (T). To clearly show each estimate, we plot the data with appropriate shift of position of the period. A model of D2c, for example, is a two-layer low viscosity model for the D″ layer, which has the viscosity of 5×10^{19} Pa s for the upper 200 km thickness and 5×10^{17} Pa s for the lower 100 km thickness (Table 2). The inset illustrates viscosity models of R5(50) and D2a.

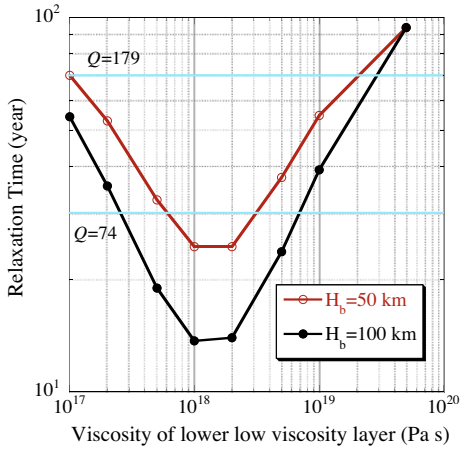

Fig. 8. Relaxation time of Chandler wobble (τ_{CW}) for two-layer low viscosity models as a function of the viscosity of the lower layer (η_b). We show the predictions for two models with the thicknesses of the lower layer (H_b) for 50 and 100 km. The total thickness of the low viscosity zone is 300 km and the viscosity of the upper layer is 5×10^{19} Pa s.

these data to the viscosity of the D″ layer in a limited case based on a background viscosity model of R0.

Here we denote the inertia elements corresponding to the non-hydrostatic geoid by ΔJ_{ij}, which are assumed to be constant for the ice age cycle examined here. If we put $\Delta A = \Delta J_{11}$, $\Delta B = \Delta J_{22}$ and $\Delta C = \Delta J_{33}$, then the Liouville equations describing the polar wander due to GIA on a convecting mantle is given by (Nakada, 2009b):

$$\left(1+\frac{\Delta C-\Delta A}{C-A}\right)m_1(t)=\frac{1}{C-A}(\delta(t)+k^L(t))*\Delta I_{13}(t)+\frac{k^T(t)}{k_f}*m_1(t) \quad (5)$$

$$\left(1+\frac{\Delta C-\Delta B}{C-A}\right)m_2(t)=\frac{1}{C-A}(\delta(t)+k^L(t))*\Delta I_{23}(t)+\frac{k^T(t)}{k_f}*m_2(t) \quad (6)$$

The terms of $(\Delta C-\Delta A)/(C-A)$ and $(\Delta C-\Delta B)/(C-A)$ have the effects stabilizing the polar wander due to the excess flattening of the Earth (Mitrovica et al., 2005; Nakada, 2009b). The values of inertia components at the present-day, which are estimated by adopting geoid expansion by Lerch et al. (1979) and the hydrostatic shape of the Earth by Nakiboglu (1982) with a hydrostatic flattening of 1/299.638 (Hager et al., 1985), are $\Delta A = -1.575 \times 10^{33}$, $\Delta B = -4.7 \times 10^{31}$ and $\Delta C = 1.622 \times 10^{33}$ kg m^2 (Nakada, 2009b). In Eqs. (2) and (3), the first terms and those for $\Delta\dot{I}_{13}$ and $\Delta\dot{I}_{23}$ are safely neglected in evaluating polar wander due to GIA (Nakada, 2009b). That is, such simplified equations describing the GIA are identical to the equations for a non-convecting mantle with $\Delta A = \Delta B = \Delta C = 0$ in Eqs. (5) and (6). The component of $\dot{m}_3(dm_3/dt)$ related to $\dot{J}_2$ is given by (Sabadini and Peltier, 1981):

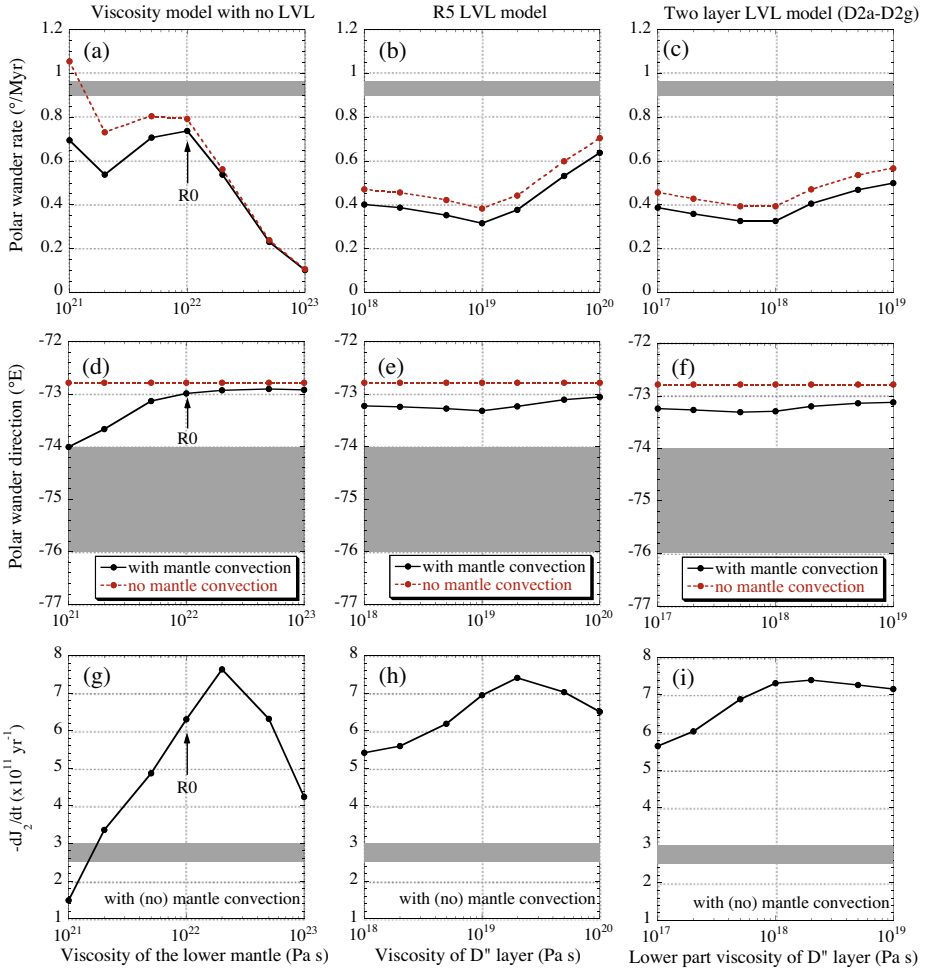

Fig. 9. Predictions of (a), (b), (c) for polar wander rate, (d), (e), (f) for polar wander direction and (g), (h), (i) for $\dot{J}_2$ based on the viscosity models with no low viscosity layer (LVL) in the mantle, R5 models (Table 1) and two-layer LVL models (D2a–D2g in Table 2) at t = 1006 kyr corresponding to the present-day. In the models with no LVL, the lithospheric (elastic) thickness and upper mantle viscosity are the same as those for R5 models, and the lower mantle viscosities are (1, 2, 5, 10, 20, 50, 100) $\times 10^{21}$ Pa s. The shaded regions show the range of the observations for the polar wander (McCarthy and Luzum, 1996) and $\dot{J}_2$ (Nerem and Klosko, 1996).

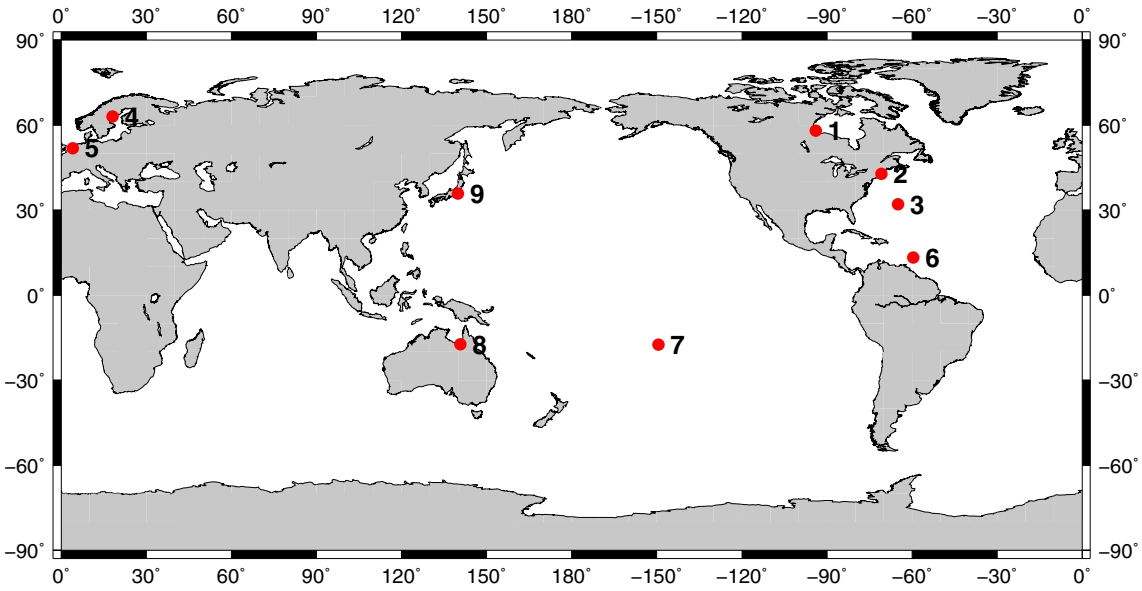

Fig. A1. Map showing sites at which relative sea-level (RSL) variations have been evaluated: (1) Churchill, (2) Boston, (3) Bermuda, (4) Angermanland, (5) Zuid_Holland, (6) Barbados, (7) Tahiti, (8) Karumba and (9) Tokyo.

$$\frac{dm_3(t)}{dt} = -\frac{1}{C}\frac{d}{dt}([\delta(t) + k^L(t)] * \Delta I_{33}(t)) \tag{7}$$

and the value of $\dot{J}_2$ is related to $\dot{m}_3$ as follows (e.g., Wu and Peltier, 1984):

$$\frac{dJ_2(t)}{dt} = -\frac{3C}{2M_e a^2}\frac{dm_3(t)}{dt} \tag{8}$$

where M_e is the mass of the Earth.

We examine the rotational quantities for the glacial cycle with 10 saw-tooth load cycles, which are characterized by a 90 kyr (1000 years) glaciation phase and by a 10 kyr deglaciation phase for each glacial cycle. The period after 1 Myr is assumed to be a postglacial phase, and the time of ~1006 kyr corresponds to the present-day. The rotation data are sensitive to both the ice model describing the gross (degree-two) melting histories during the last deglaciation and rheological structure of the Earth (e.g., Nakada and Okuno, 2003). We therefore adopt ICE-3G model (Tushingham and Peltier, 1991) to only examine the sensitivity of the rotation data to the viscosity of the D″ layer. The values of ΔI_{13}, ΔI_{23} and ΔI_{33} at the glacial maximum are: $\Delta I_{13} = -6.91 \times 10^{31}$, $\Delta I_{23} = 2.23 \times 10^{32}$ and $\Delta I_{33} = -8.11 \times 10^{32}$ kg m^2 (Nakada, 2009b).

Fig. 9 shows the predictions of the polar wander rate, polar wander direction and $\dot{J}_2$ for models with no low viscosity layer (LVL) in the mantle, R5 models and two-layer LVL models (D2a–D2g) at t = 1006 kyr corresponding to the present-day. In the models with no LVL, the lithospheric (elastic) thickness and upper mantle viscosity are the same as those for R5 models, and the lower mantle viscosities are (1, 2, 5, 10, 20, 50, 100) × 10^{21} Pa s. The results for viscosity models with no LVL are shown because we examine the importance of the viscosity structure of the D″ layer by comparing the results for R5 and two-layer LVL models with those without LVL. We also show the polar wander predictions (rate and direction) for both a non-convecting mantle and convecting one, and only discuss the results for a convecting mantle. The shaded regions show the range of the observations for the polar wander (McCarthy and Luzum, 1996) and $\dot{J}_2$ (Nerem and Klosko, 1996).

The polar wander direction for R5 and two-layer LVL models is similar to that for R0, and the amount of change for adopted low D″ viscosity range is rather smaller than that for no LVL model and also that for the observation uncertainty. That is, the polar wander direction is insensitive to the viscosity structure of the D″ layer. However, the polar wander rate and $\dot{J}_2$ are sensitive to the viscosity structure of the D″ layer. The amount of change in the polar wander rate for R5 and two-layer models is larger than ~0.2° Myr^{-1}, which is about the half of that for no LVL model (Fig. 9a) and also much larger than the observation uncertainty. That is, the polar wander rate due to GIA is highly sensitive to both the lower mantle viscosity and the viscosity of the D″ layer. This conclusion is also true for the predicted $\dot{J}_2$. Although we only discuss the sensitivities to the viscosity of the D″ layer based on a background model R0, it is necessary to take into account the effects of the low viscosity D″ layer when we examine the viscosity structure, recent melting events and convective processes based on these observed secular rotational variations.

8. Concluding remarks

D″ layer of the Earth's mantle, the lowermost layer in the Earth's mantle, plays an important role in the dynamics and evolution of the Earth. Among others, its rheological properties controls a number of geodynamic processes, but a robust estimate of its viscosity has been hampered by the lack of relevant observations. A commonly used analysis of geophysical signals in terms of heterogeneity in seismic wave velocities (Forte and Mitrovica, 2001) suffers from major uncertainties in the velocity-to-density conversion factor (Karato and Karki, 2001; Karato, 2008), and the glacial rebound observations for the relative sea level have little sensitivity to the viscosity of the mantle deeper than ~1200 km (Mitrovica and Peltier, 1991). However, there is no doubt that the geoid information is highly sensitive to the low viscosity of the D″ layer (Hager et al., 1985; Cadek and Fleitout, 2006; Tosi et al., 2009), and therefore the results for the low viscosity inferred from the geoid information (Tosi et al., 2009) and the present study may give us some more information about mineral physics of the D″ region.

In this study, we examined the sensitivities of the viscosity structure to the decay time of the Chandler wobble and semi-diurnal to 18.6 years tidal deformation by taking into account the GIA constraints for the relative sea level. The decay time of Chandler wobble provides an important constraint on the effective viscosity of the D″ layer with the thickness of ~300 km. On the other hand, the tidal deformation is very sensitive to the viscosity of the bottom part of the D″ layer with ~100 km. These deformations combined with the GIA constraints suggest that the effective viscosity of the D″ layer (~300 km thickness) is 10^{19}–10^{20} Pa s,

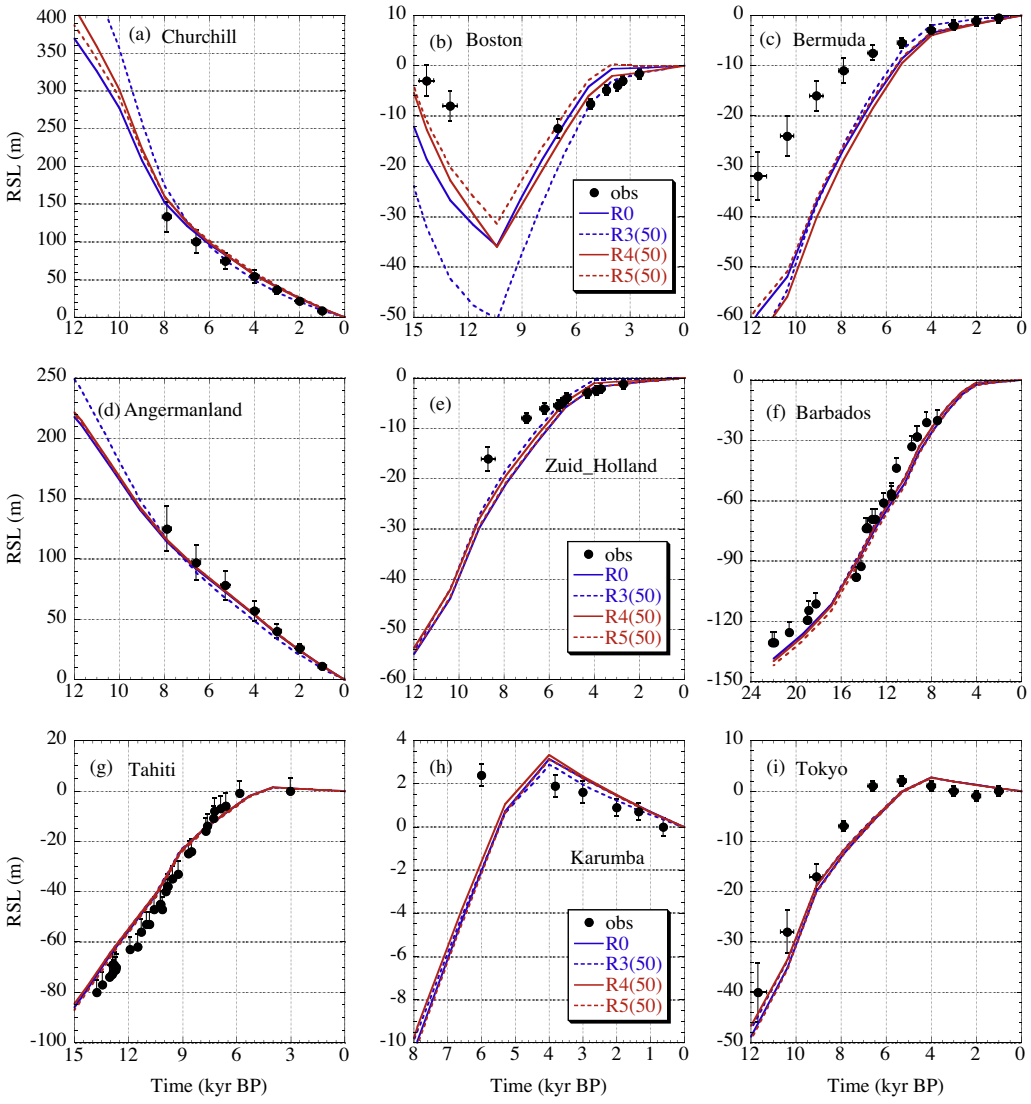

Fig. A2. Relative sea-level variations for the sites shown in Fig. A1 based on the ice model of ICE-3G (Tushingham and Peltier, 1991) and viscosity models for R0, R3(50), R4(50) and R5(50) (see Table 1). The data source for observed RSLs is: http://www.ncdc.noaa.gov/paleo/recons.html.

and also the effective viscosity of the bottom part of the D″ layer (∼100 km thickness) is less than 10^{18} Pa s. Such a viscosity structure of the D″ layer is a natural consequence of a steep temperature gradient in the D″ layer inferred from the double-crossing of seismic rays of the phase boundary between perovskite and post-perovskite (Hernlund et al., 2005).

The inferred low viscosity of the D″ layer has a few geodynamic implications. For instance, a low viscosity in that layer implies vigorous small-scale convection (the local Rayleigh number will be 2×10^5 for a layer of 200 km thickness with 10^{19} Pa s). This will facilitate the material exchange between the core and mantle. However, a low viscosity also implies a low stress associated with convection. Hernlund and Jellinek (2010) argued that melt with a different density than the surrounding materials could be retained in the D″ layer due to the influence of pressure gradients caused by the convection in the adjacent layer. If the viscosity of the D″ layer is as low as the present study suggests, mechanisms other than partial melting would be needed to explain the ultra-low velocity regions.

Acknowledgments

We thank J. Okuno for computing relative sea-level changes and two anonymous reviewers for their helpful comments. This work was partly supported by the Japanese Ministry of Education, Science and Culture (Grand-in-Aid for Scientific Research No. 22540440)

Appendix A

In this paper, we assume that the relative sea-level (RSL) variations in the postglacial phase, which have been used to infer the rheological structure of the mantle (e.g., Nakada and Lambeck, 1987; Tushingham and Peltier, 1991), have little sensitivity to the viscosity of the mantle deeper than ∼1200 km depth (Mitrovica and Peltier, 1991). Here we examine this assumption by evaluating the RSL variations based on the ice model of ICE-3G (Tushingham and Peltier, 1991) and the viscosity models adopted in this paper. The RSL variations are equally sensitive to both the ice model describing the melting histories of the ice sheets and the rheological structure of the mantle (Nakada and Lambeck, 1987). We therefore adopt the ICE-3G model to only examine the sensitivity of RSL to the viscosity structure with a low viscosity layer (LVL) in the lower mantle. The RSL variations are computed based on the method by Okuno and Nakada (2001).

The thickness of the elastic lithosphere is 100 km and the upper mantle viscosity is 10^{21} Pa s. The lower mantle viscosity except for

the LVL is assumed to be 10^{22} Pa s. We adopt the LVL with a thickness of 300 km and viscosity of 5×10^{19} Pa s, and compute the RSL variations based on the viscosity models with a LVL layer for a depth range of 791–1091 km depth (R3), 1091–1391 km depth, 1391–1691 km depth, 1691–1991 km depth (R4), 1991–2291 km depth, 2291–2591 km depth and 2591–2891 km depth (R5). Here we only show the results for R0 (with no LVL), R3(50), R4(50) and R5(50) (see Table 1) in this appendix, because the conclusion for the sensitivities of the RSLs to the LVL does not change even if we show the results for other viscosity models.

Fig. A2 shows the observations and predictions for the sites shown in Fig. A1. In the predictions for Churchill and Angermanland located at the central regions of the former ice sheets, the RSLs in the late glacial phase (before ~7 kyr BP) for R3(50) are rather different from those for R0 with no LVL, but those for other LVL models are similar to those for R0. The tendency can be clearly seen for the RSLs at Boston near the edge region of the Laurentide ice sheet. The RSLs at these three sites for a model with LVL for 1391–1691 km depth, which we do not show here, are similar to those for R4(50). The RSLs at other six sites for R4(50) and R5(50) are nearly identical to those for R0. Summarizing these results, we conclude that the GIA observations for the relative sea level variations during the postglacial phase have little sensitivity to the viscosity of the mantle deeper than ~1200 km as indicated by Mitrovica and Peltier (1991).

References

Amin, K.E., Mukherjee, A.K., Dorn, J.E., 1970. A universal law for high-temperature diffusion controlled transient creep. J. Mech. Phys. Solids 18, 413–426.

Ammann, M.W., Brodholt, J.P., Wookey, J., Dobson, 2010. First-principles constraints on diffusion in lower-mantle minerals and week D″ layer. Nature 465, 462–465.

Aoyama, Y., Naito, I., 2001. Atmospheric excitation of the Chandler wobble, 1983–1998. J. Geophys. Res. 106, 8941–8954.

Benjamin, D., Wahr, J., Ray, R.D., Egbert, G.D., Sesai, S.D., 2006. Constraints on mantle anelasticity from geodetic observations, and implications for the J_2 anomaly. Geophys. J. Int. 165, 3–16.

Buffett, B.A., 1992. Constraints on magnetic energy and mantle conductivity from the forced nutations of the Earth. J. Geophys. Res. 97, 19581–19597.

Buffett, B.A., 1997. Geodynamic estimates of the viscosity of the Earth's inner core. Nature 388, 571–573.

Buffett, B.A., Mathews, P.M., Herring, T.A., 2002. Modeling of nutation and precession: effects of electromagnetic coupling. J. Geophys. Res. 107. doi:10.1029/2000JB000056.

Cadek, O., Fleitout, L., 2006. Effect of lateral viscosity variations in the core–mantle boundary region on predictions of the long-wavelength geoid. Stud. Geophys. Geod. 50, 217–232.

Dickman, S.R., 1977. Secular trend of the Earth's rotation pole: consideration of motion of the latitude observatories. Geophys. J. R. Astr. Soc. 51, 229–244.

Dickman, S.R., Nam, Y.S., 1998. Constraints on Q at long periods from Earth's rotation. Geophys. Res. Lett. 25, 211–214.

Dziewonski, A.M., Anderson, D.L., 1981. Preliminary reference Earth model (PREM). Phys. Earth Planet. Inter. 25, 297–356.

Forte, A.M., 2007. Constraints on seismic models from other disciplines–implications for mantle dynamics and composition. In: Romanowicz, B., Dziewonski, A. (Eds.), Treatise on Geophysics vol. 1. Seismology and Structure of the Earth, Elsevier, pp. 805–858.

Forte, A.M., Mitrovica, J.X., 2001. Deep-mantle high viscosity flow and thermochemical structure inferred from seismic and geodynamic data. Nature 410, 1049–1056.

Furuya, M., Chao, B.F., 1996. Estimation of period and Q of the Chandler wobble. Geophys. J. Int. 127, 693–702.

Furuya, M., Hamano, Y., Naito, I., 1996. Quasi-periodic wind signal as a possible excitation of Chandler wobble. J. Geophys. Res. 101, 25537–25546.

Getting, I.C., Dutton, S.J., Burnly, P.C., Karato, S., Spetzler, H.A., 1997. Shear attenuation and dispersion in MgO. Phys. Earth Planet. Inter. 99, 249–257.

Gross, R.S., 2005. The observed period and Q of the Chandler wobble. In: Plag. H-P., Chao, B.F., Gross, R.S., Dam, T. (Eds.), Forcing of Polar Motion in the Chandler Frequency Band: A Contribution to Understanding interannual Climate Change, vol. 24, Cahiers du Centre Européen de Géodynamique et se Séismologie, pp. 31–37.

Gross, R.S., 2007. Earth rotation variations–long periods. In: Herring, T. (Ed.), Treatise on Geophysics vol. 3. Geodesy, Elsevier, pp. 239–294.

Gross, R.S., Fukumori, I., Menemenlis, D., 2003. Atmospheric and oceanic excitation of the Earth's wobbles during 1980–2000. J. Geophys. Res. 108. doi:10.1029/2002JB002143.

Hager, B.H., 1984. Subducted slabs and the geoid: constraints on mantle rheology and flow. J. Geophys. Res. 89, 6003–6015.

Hager, B.H., Clayton, R.W., Richards, M.A., Comer, R.P., Dziewonski, A.M., 1985. Lower mantle heterogeneity, dynamic topography and the geoid. Nature 313, 541–545.

Hernlund, J.W., Thomas, C., Tackley, P.J., 2005. A dounbling of the post-perovskite phase boundary and structure of the Earth's lowermost mantle. Nature 434, 882–886.

Hernlund, J.W., Jellinek, A.M., 2010. Dynamics and structure of a stirred partially molten ultralow-velocity zone. Earth Planet. Sci. Lett. 296, 1–8.

Ivins, E.R., Sammis, C.G., 1995. On lateral viscosity contrast in the mantle and the rheology of low-frequency geodynamics. Geophys. J. Int. 123, 305–322.

Jackson, I., 2007. Properties of rocks and minerals – physical origins of anelasticity and attenuation in rock. In: Price, G.D. (Ed.), Treatise on Geophysics vol. 2. Mineral Physics, Elsevier, pp. 493–525.

Jackson, I., Faul, U.H., 2010. Grainsize-sensitive viscoelastic relaxation in olivine: towards a robust laboratory-based model for seismological application. Phys. Earth Planet. Inter. 183, 151–163.

Karato, S., 1998. A dislocation model of seismic wave attenuation and velocity dispersion and microcreep of the solid Earth: Harold Jeffreys and the rheology of the solid Earth. Pure Appl. Geophys. 153, 239–256.

Karato, S., 2008. Deformation of earth materials: an introduction to the rheology of solid earth. Cambridge University Press, Cambridge.

Karato, S., 2010a. Rheology of the Earth's mantle: a historical review. Gondwana Res. 18, 17–45.

Karato, S., 2010b. The influence of anisotropic diffusion on the high-temperature creep of a polycrystalline aggregate. Phys. Earth Planet. Inter. 183, 468–472.

Karato, S., 2011. Water distribution across the mantle transition zone and its implications for global material circulation. Earth Planet. Sci. Lett. 301, 413–423.

Karato, S., Spetzler, H.A., 1990. Defect microdynamics in minerals and solid state mechanisms of seismic wave attenuation and velocity dispersion in the mantle. Rev. Geophys. 28, 399–421.

Karato, S., Karki, B.B., 2001. Origin of lateral heterogeneity of seismic wave velocities and density in Earth's deep mantle. J. Geophys. Res. 106, 21771–21783.

Lakki, A., Schaller, R., Carry, C., Benoit, 1998. High temperature anelastic and viscoelastic deformation of fine-grained MgO-doped Al_2O_3. Acta Materialia 46, 689–700.

Lambeck, K., 1980. The Earth's Variable Rotation: Geophysical Causes and Consequences. Cambridge University Press, Cambridge.

Lambeck, K., Nakiboglu, S.M., 1983. Long-period Love numbers and their frequency dependence due to dispersion effects. Geophys. Res. Lett. 10, 857–860.

Lambeck, K., Johnston, P., Smither, C., Nakada, M., 1996. Glacial rebound of the British Isles III. Constraints on mantle viscosity. Geophys. J. Int. 125, 340–354.

Lay, T., Williams, Q., Garnero, E.J., 1998. The core–mantle boundary layer and deep Earth dynamics. Nature 392, 461–468.

Lerch, F.J., Klosko, S.M., Laubscher, R.E., Wagner, C.A., 1979. Gravity model improvement using Geos 3 (GEM-9 and 10). J. Geophys. Res. 84, 3897–3916.

McCarthy, D.D., Luzum, B.J., 1996. Path of the mean rotational pole from 1899 to 1994. Geophys. J. Int. 125, 623–629.

Mitrovica, J.X., 1996. Haskell [1935] revisited. J. Geophys. Res. 101, 555–569.

Mitrovica, J.X., Peltier, W.R., 1991. Radial resolution in the inference of mantle viscosity from observations of glacial isostatic adjustment. In: Sabadini, R., Lambeck, K., Boschi, E. (Eds.), Glacial Isostasy, Sea-Level and Mantle Rheology. Kluwer Academic Publisher, Dordrecht, pp. 63–78.

Mitrovica, J.X., Forte, A.M., 2004. A new inference of mantle viscosity based upon joint inversion of convection and glacial isostatic adjustment data. Earth Planet. Sci. Lett. 225, 177–189.

Mitrovica, J.X., Wahr, J., Matsuyama, I., Paulson, A., 2005. The rotational stability of an ice-age earth. Geophys. J. Int. 161, 491–506.

Mitorovica, J.X., Wahr, J., Matsuyama, I., Paulson, A., Tamisiea, M.E., 2006. Reanalysis of ancient eclipse, astronomic and geodetic data: a possible route to resolving the enigma of global sea-level rise. Earth Planet. Sci. Lett. 243, 390–399.

Munk, W.H., MacDonald, G.J.F., 1960. The Rotation of the Earth: a Geophysical Discussion. Cambridge University Press, Cambridge.

Nakada, M., 2002. Polar wander caused by the Quaternary glacial cycles and fluid Love number. Earth Planet. Sci. Lett. 200, 159–166.

Nakada, M., 2006. Axial and equatorial rotations of the Earth's cores associated with the Quaternary ice age. Phys. Earth Planet. Inter. 154, 113–147.

Nakada, M., 2009a. Earth's rotational variations by electromagnetic coupling due to core surface flow on a timescale of 1 year for geomagnetic jerk. Geophys. J. Int. 179, 521–535.

Nakada, M., 2009b. Polar wander of the Earth associated with the Quaternary glacial cycle on a convecting mantle. Geophys. J. Int. 179, 569–578.

Nakada, M., 2011. Earth's rotational variations due to rapid surface flows at both boundaries of the outer core. Geophys. J. Int. 184, 235–246.

Nakada, M., Lambeck, K., 1987. Glacial rebound and relative sea-level variations: a new appraisal. Geophys. J. R. Astr. Soc. 90, 171–224.

Nakada, M., Lambeck, K., 1989. Late Pleistocene and Holocene sea-level change in the Australian region and mantle rheology. Geophys. J. 96, 497–517.

Nakada, M., Okuno, J., 2003. Perturbations of the Earth's rotation and their implications for the present-day mass balance of both polar ice caps. Geophys. J. Int. 152, 124–138.

Nakiboglu, S.M., 1982. Hydrostatic theory of the Earth and its mechanical implications. Phys. Earth Planet. Inter. 28, 302–311.

Nerem, R.S., Klosko, S.M., 1996. Secular variations of zonal harmonics and polar motion as geophysical constraint. In: Rapp, R.H., Cazenave, A.A., Nerem, R.S. (Eds.), Global Gravity Field and its Temporal Variations. Springer, New York, pp. 152–163.

Okuno, J., Nakada, M., 2001. Effects of water load on geophysical signals due to glacial rebound and implications for mantle viscosity. Earth Planets Space 53, 1121–1135.

Peltier, W.R., 1974. The impulse response of a Maxwell Earth. Rev. Geophys. Space Phys. 12, 649–669.

Peltier, W.R., 1988. Global sea level rise and Earth rotation. Science 240, 895–901.

Ray, R.D., Eanes, R.J., Lemoine, F.G., 2001. Constraints on energy dissipation in the Earth's body tide from satellite tracking and altimetry. Geophys. J. Int. 144, 471–480.

Ricard, Y., Sabadini, R., 1990. Rotational instabilities of the Earth induced by mantle density anomalies. Geophys. Res. Lett. 17, 627–630.

Sabadini, R., Peltier, W.R., 1981. Pleistocene deglaciation and the Earth's rotation: implications for mantle viscosity. Geophys. J. R. Astr. Soc. 66, 553–578.

Sabadini, R., Yuen, D.A., Widmer, R., 1985. Constraints on short-term mantle rheology from the J_2 observation and dispersion of the 18.6 y tidal Love number. Phys. Earth Planet. Inter. 38, 235–249.

Sasao, T., Okubo, S., Saito, M., 1980. A simple theory on the dynamical effects of a stratified fluid core upon nutational motion of the Earth. In: Federov, E.P., Smith, M.L., Bender, P.L. (Eds.), Proceedings of IAU Symposium 78. R. Reidel, Hingham, MA, USA, pp. 165–183.

Smith, M.L., Dahlen, F.A., 1981. The period and Q of the Chandler wobble. Geophys. J. R. Astr. Soc. 64, 223–281.

Steinberger, B.M., O'Connell, R.J., 1997. Changes of the Earth's rotation axis inferred from advection of mantle density heterogeneities. Nature 387, 169–173.

Tosi, N., Cadek, O., Martinec, Z., Yuen, D.A., Kaufmann, G., 2009. Is the long-wavelength geoid sensitive to the presence of postperovskite above the core–mantle boundary? Geophys. Res. Lett., 36, doi:10.1029/2008GL036902.

Tushingham, A.M., Peltier, W.R., 1991. ICE-3G: a new global model of late Pleistocene deglaciation based upon geophysical predictions of post-glacial relative sea level change. J. Geophys. Res. 96, 4497–4523.

Wahr, J.M., Bergen, Z., 1986. The effects of mantle elasticity on nutation, Earth tides, and tidal variations in rotation rate. Geophys. J. R. Astr. Soc. 87, 633–668.

Wilson, C.R., Haubrich, R.A., 1976. Meteorological excitation of the Earth's wobble. Geophys. J. R. Astr. Soc. 46, 707–743.

Wilson, C.R., Vicente, R.O., 1990. Maximum likelihood estimates of polar motion parameters. In: McCarthy, D.D., Carter, W.E. (Eds.), Variations in Earth Rotation, AGU Geophys. Monogr. 59. American Geophysical Union, pp. 151–155.

Wu, P., Peltier, W.R., 1984. Pleistocene deglaciation and the Earth's rotation: a new analysis. Geophys. J. R. Astr. Soc. 76, 753–791.

Yamazaki, D., Karato, S., 2001. Some mineral physics constraints on the rheology and geothermal structure of Earth's lower mantle. Am. Mineral. 86, 385–391.